Fabrication and Thermoelectric Properties of p-$Bi_{0.4}Sb_{1.6}Te_{3.4}$ and n-Bi_2Te_3 for Thermal Sensors

Surasak Ruamruk [a,*]

[a] *Program of Physics, Faculty of Science and Technology, Sakon Nakhon Rajabhat University, Sakon Nakhon, 47000, Thailand*

Received 24 April 2019; Revised 15 July 2019; Accepted 31 July 2019

Abstract

We optimized a low signal the thermal sensor of p-Sb_2Te_3 by synthesized p-$Bi_{0.4}Sb_{1.6}Te_{3.4}$ from Bi, Sb and Te powder using planetary ball mill and hot press methods to obtain bulk samples. The thermoelectric (TE) properties and crystal structure of bulk samples were investigated by ZEM-3 and XRD method. The electrical conductivity, Seebeck coefficient, thermal conductivity and dimensionless figure of merit of p-$Bi_{0.4}Sb_{1.6}Te_{3.4}$ and n-Bi_2Te_3 samples were increased with increasing temperature range from 300 − 550 K in He atmosphere. The thermal sensor of p-$Bi_{0.4}Sb_{1.6}Te_{3.4}$ and n-Bi_2Te_3 thermoelectric cell has similarly signal K type thermocouple.

KEYWORDS: Thermoelectric sensor; Thermoelectric device; Thermoelectric materials; Thermocouple
*Corresponding authors; E-mail: ruamruk2537@gmail.com

Introduction

The most industries have waste heat from compressor and condenser, were high-temperature equipment cause damage. However, the waste heat can recycle for increase thermal efficiency and cost saving by thermoelectric devices. So, thermoelectric devices can detect temperature or sensitivity form waste heat to reduce erosion of equipment and generated electrical power. Recently, the thermal sensor can measure signal or physical quantities such as temperature, voice, light, mechanical strength, pressure, displacement, speed, accelerate, fluid and flow rates. The thermoelectric devices have been changed heat into electricity as well as it much interested in their potential application in power generated and refrigerate [1 – 2]. The performance of TE materials related to parameter called the dimensionless figure of merit: $ZT = S^2T/\rho(\kappa_e+\kappa_L)$, where S is the Seebeck coefficient, T is absolute temperature, ρ is electrical resistivity, κ_e is the thermal conductivity and κ_L is the lattice thermal conductivity [3 – 4]. Bismuth telluride (Bi_2Te_3) is popular materials and the best TE materials operating at a close low temperature application to daily life and industrial work. The crystal structure of these materials is a hexagonal structure, space group number 166 and lattice parameter a = 4.38 Å and c = 30.48 Å [5]. The researchers have synthesis Bi_2Te_3 various methods such as solid state reaction (SSR), spark plasma sintering (SPS) and hot press (HP) . Dan-Di Li et al. (2011) reported and characterized TE properties of p-type Bi_2Te_3 and Sb_2Te_3 prepared by SPS method [6]. The σ significantly increased and κ decreased obtain the maximum ZT = 1.33 at 398 K [6]. The SPS method included the hot deformation process, leading to point defect engineering (ZT = 1.30 at 380 K) [7]. The HP method used ball milled nano powders (ZT = 1.40 at 373 K) [8]. The SPS of melt spun ribbons (ZT = 1.56 at 300 K) [9]. A melt spun, SPS process of $Bi_xSb_{2-x}Te_3$ with excess Te resulting in dens dislocation arrays though liquid phase compaction ZT = 1.86 at 320 K [10]. However, many studies have shown the TE can be wonderfully integrated with various sensors. Haiyan Liu et al. (2018) reported cellulose based TE generator for harvesting human body energy shown the output power 130.60 nW [11]. J.J. Kuchle et al. (2014) reported self-powered wireless TE sensors shown the maximum different temperature 191 °C and output voltage 2.57 V [12]. Zhenxiang Yi et al. (2015) analyzed effect on the TE power sensor shown the surrounding temperature recorded under 50 mW [13]. Yong Jun Kim et al. (2018) reported high-performance self-powered wireless sensor by flexible TE generator and minimum voltage set to 3.78 V [14]. Huan et al. (2018) reported cellulose-based TE sponge towards wearable pressure sensor and

energy harvesting and the output voltage increases proportionally with temperature difference of 0.5 mV at 30 K [15].

In this we proposed a new thermal sensor by synthesized p-$Bi_{0.4}Sb_{1.6}Te_{3.4}$ and n-Bi_2Te_3 TE materials and measured thermoelectric properties of these materials. We fabricated thermal sensor from p-$Bi_{0.4}Sb_{1.6}Te_{3.4}$ and n-Bi_2Te_3 cell sensitive with Arduino program for probabilities thermal sensor application industry machines.

Materials and Methods

Materials

The polycrystalline of p-$Bi_{0.4}Sb_{1.6}Te_{3.4}$ and n-Bi_2Te_3 thermoelectric materials were synthesized by hot pressed from Bismuth (Bi), Antimony (Sb) and Telluride (Te) powders (< 99% purity) in a cylindrical graphite die (internal diameter of 4 cm) at 673 K under 24 MPa for 1 h in vacuum [16]. The crystal structure of the thermoelectric materials was analyzed by using an X-ray diffractometer (XRD-6100 Shimadzu, Japan) at room temperature using CuK_α radiation (λ = 1.5406 Å) in the range of 2θ = 20 – 70° mode. The ρ and s were simultaneously measured by TE measurement system (ZEM-3 ADVANCE RIKO) in helium atmosphere at the temperature range of 300 – 550 K. The κ was calculated by the relation (1);

$$\kappa = \frac{\dot{Q}}{A\Delta T} \quad (1)$$

where $\dot{Q}$ the amount of heat following of the sample, A is the cross-section area of the sample and ΔT is the temperature difference between thermocouples.

Device Fabrication and Evaluation

The circuit collected and transmitted data of four main elements: TE cell to ESP8266 module, storage capacitors, controller transmitter and a receiver. A circuit diagram with a flowchart of the various elements and the actual breadboarded circuit, as shown in Fig. 2(a). The Arduino Nano is a small, complete, and breadboard-friendly board based on the ATmega328P. We used Arduino Nano for receiver from TE cell and send the output voltage in Bluetooth signal to ESP8226, as shown in Fig. 2(b). The output voltage was converted signal to be temperature by ESP8266 module and send to display in this program.

The TE cell was fabricated by using p-$Bi_{0.4}Sb_{1.6}Te_{3.4}$ and n-Bi_2Te_3 bulk materials cutting size of 2.5 × 2.5 × 3 mm^3 constructs Zinc electrodes in ceramic tubes size 10 cm^3 to a body of the thermal sensor, as shown in Fig. 1(a). ESP8266 module was an impressive, low cost WI-FI module suitable for adding WI-FI functionality to an existing microcontroller project via a UART serial connection [17] and using Arduino program to support. The selection board Arduino for working process of the program, as shown in Fig. 1(b).

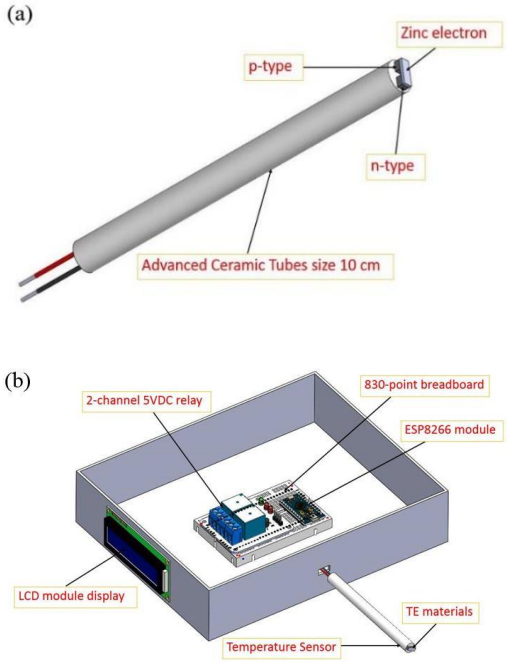

Fig. 1 Schematic diagram of (a) thermal sensor (b) circuit for convert signal

Circuit Design

The circuit collected and transmitted data of four main elements: TE cell to ESP8266 module, storage capacitors, controller transmitter and a receiver. A circuit diagram with a flowchart of the various elements and the actual breadboarded circuit, as shown in Fig. 2(a). The Arduino Nano is a small, complete, and breadboard-friendly board based on the ATmega328P. We used Arduino Nano for receiver from TE cell and send the output voltage in Bluetooth signal to ESP8226, as shown in Fig. 2(b). The output voltage was converted signal to be temperature by ESP8266 module and send to display in this program.

Results and Discussion

The measured relationship between diffraction angle and X-ray intensity of

sintered Bi_2Te_3 at room temperature is shown in Fig. 3. The XRD patterns of n-Bi_2Te_3 sample show the single γBi_2Te_3 phase with a rhombohedra structure space group in $R\bar{3}m$ correspond with the standard patterns of Bi_2Te_3 (ICDD PDF 00-015-0863).

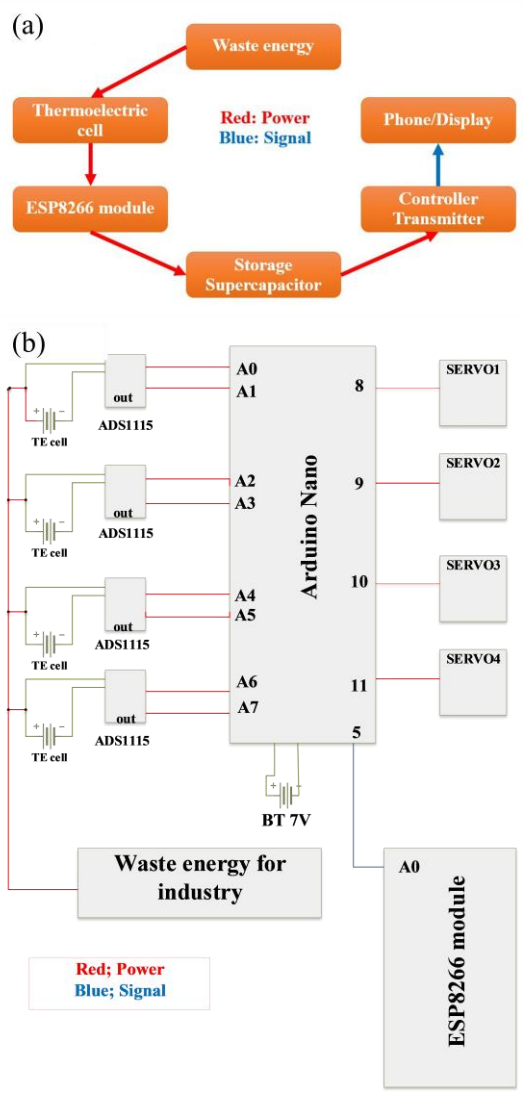

Fig. 2 Schematic diagram of (a) power and signal through circuit (b) power and signal through circuit by Visio Professional

The measured relationship between diffraction angle and X-ray intensity of sintered $Bi_{0.4}Sb_{1.6}Te_3$ at room temperature is shown in Fig. 4. The XRD patterns of $Bi_{0.4}Sb_{1.6}Te_3$ sample show all the diffraction peaks can be indexed according the crystallographic structure of p-$Bi_{0.4}Sb_{1.6}Te_{3.4}$ rhombohedral crystal structure of space group R3m correspond with the standard XRD patterns of p-Sb_2Te_3 (ICDD PDF 00-049-1713). The (0 1 5), (1 0 10) and (0 0 15) peaks are the dominant peaks, which indicate a preferential growth of the grains along these directions. The peak at around 27.6° from the Te element confirms that the sample is Te-rich [18].

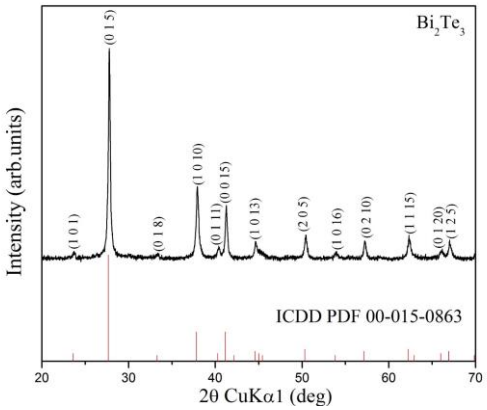

Fig. 3 The XRD pattern together with ICDD PDF 00-015-083 of Bi_2Te_3 bulk sample

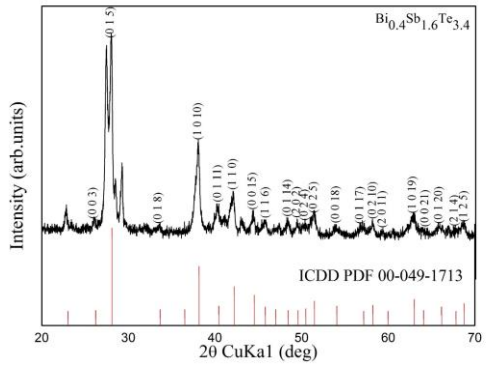

Fig. 4 The XRD patterns together with ICDD PDF 00-049-1713 of $Bi_{0.4}Sb_{1.6}Te_{3.4}$ bulk sample

The temperature dependence range of 325 – 525 K on the S of the Bi_2Te_3 bulk prepared by hot-press at 673 K for 1 h in Ar atmosphere and compared with literature data are shown in Fig 5(a). The S of n-Bi_2Te_3 shows negative value indicate that an n-type and decreased with increasing temperature from – 155.92 μV K^{-1} at 325 K to – 123.65 μV K^{-1} at 525 K correspond with (Go-Eun Lee et al. 2014) [16]. The ρ of Bi_2Te_3 sample decreased with increasing temperature indicate the semiconductor behavior. The ρ value of the Bi_2Te_3 sample shows 20.35 × 10^{-5} Ω m at 325 K to 13.89 × 10^{-5} Ω m at 525 K, as shown in Fig. 5(b). Moreover, the evaluated power factor (PF) of the Bi_2Te_3 sample at temperature range of

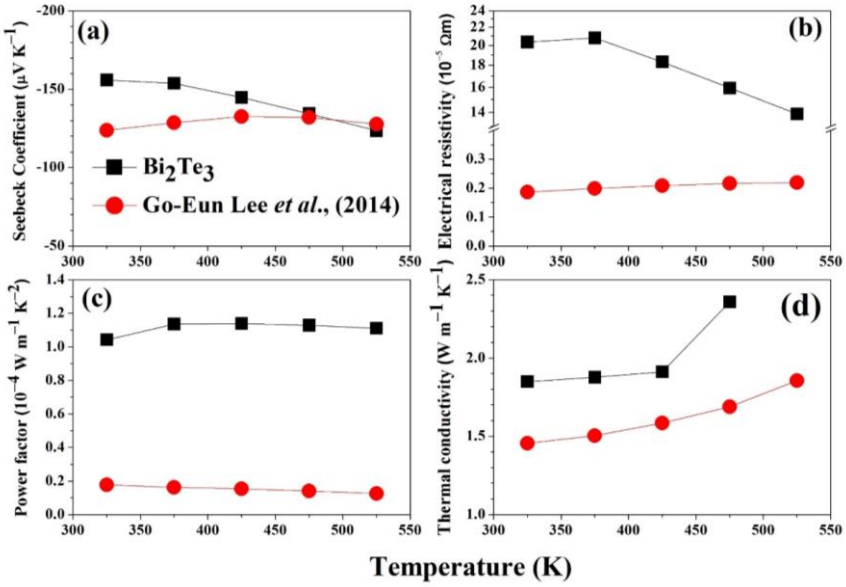

Fig. 5 (a) Temperature dependent on Seebeck coefficient of Bi_2Te_3 (b) electrical conductivity, (c) power factor and (d) thermal conductivity compared with Go-Eun Lee *et al.* [16].

325 – 525 K. The *PF* values of the n-Bi_2Te_3 sample increased with increasing temperature from 1.04 × 10^{-4} W m^{-1} K^{-2} at 325 K to 1.11 × 10^{-4} W m^{-1} K^{-2} at 525 K, as shown in Fig. 5(c). The κ of Bi_2Te_3 sample increased with increasing temperature from 1.85 W m^{-1} K^{-1} at 325 K to 2.35 W m^{-1} K^{-1} at 475 K, as shown in Fig. 5(d). However, the κ of n-Bi_2Te_3 values had higher than that of literature data (Go-Eun Lee et al. 2014) [16].

Temperature dependence on the *S* of the $Bi_{0.4}Sb_{1.6}Te_{3.4}$ sample at the temperature range of 325 – 525 K compared with literature data, as shown in Fig 6(a). The *S* values of $Bi_{0.4}Sb_{1.6}Te_{3.4}$ show positive value indicate that an p-type and increased with increasing temperature from 156.34 μV K^{-1} at 325 K to 159.02 μV K^{-1} at 375 K. However, these values are lower than that of the samples [18] but p-$Bi_{0.4}Sb_{1.6}Te_{3.4}$ sample had *S* value similar with Yong Jun Kim *et al.* [14]. The ρ of $Bi_{0.4}Sb_{1.6}Te_{3.4}$ sample increased with increasing temperature indicate of semiconductor behavior from 0.04 mΩ m at 325 K to 0.05 mΩ m at 525 K. However, these

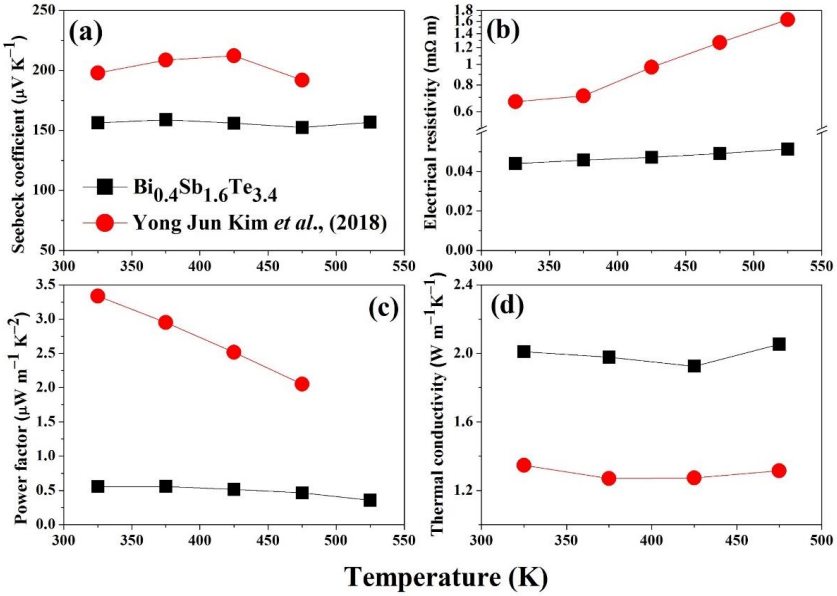

Fig. 6 (a) Temperature dependence on Seebeck coefficient of p-$Bi_{0.4}Sb_{1.6}Te_{3.4}$ (b) electrical conductivity, (c) power factor and (d) thermal conductivity compared with Yong Jun Kim *et al.* [14].

values are lower than that of the reference, as show in Fig. 6(b). The *PF* of p-$Bi_{0.4}Sb_{1.6}Te_{3.4}$ sample decreased with increasing temperature from 0.06 μW m^{-1} K^{-2} at 325 K to 0.04 μW m^{-1} K^{-2} at 525 K, as shown in Fig. 6(c).

The κ of p-$Bi_{0.4}Sb_{1.6}Te_{3.4}$ sample at the temperature range of 325 – 475 K increased with increasing temperature from 2.01 W m^{-1} K^{-1} at 325 K to 2.05 W m^{-1} K^{-1} at 475 K, as shown in Fig. 6(d). Temperature dependence on *ZT* of n-Bi_2Te_3 sample compared with Go-Eun Lee *at al*. [16], as shown in Fig. 7. The evaluated *ZT* from S , ρ and κ values at temperature range of 325 – 475 K shows 0.02 at 325 K to 0.03 at 475 K increased with increasing temperature but it lower than Go-Eun Lee *et al*. [16] at the same temperature range.

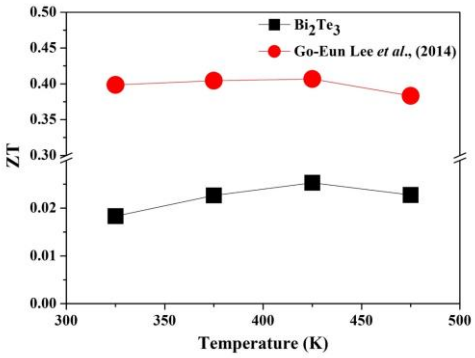

Fig. 7 Temperature dependence on *ZT* for sintered Bi_2Te_3 bulk sample compared with Go-Eun Lee *et al.* [16].

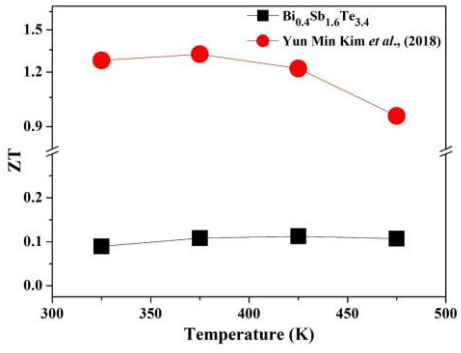

Fig. 8 Temperature dependence on *ZT* of sintered $Bi_{0.4}Sb_{1.6}Te_{3.4}$ bulk sample compared with Yun Min Kim *et al.* [14].

Temperature 325 – 475 K dependence on *ZT* dependence of p-$Bi_{0.4}Sb_{1.6}Te_{3.4}$ sample compared with Xi and Fan et al. (2015) [19], as shown in Fig. 8. The *ZT* of p-$Bi_{0.4}Sb_{1.6}Te_{3.4}$ sample shows 0.09 at 325 K to 0.1 at 475 K and increased with increasing temperature. The different temperature dependence on voltage value of TE cell, as shown in Fig. 9. The voltage output shows 0. 03 mV at 49 K per a pair and increased with increasing temperature. The temperature dependence on time of the thermal sensor together with thermocouple type K, as shown in Fig. 10. The thermal sensor shows significantly value correspond with standard of thermocouple type K.

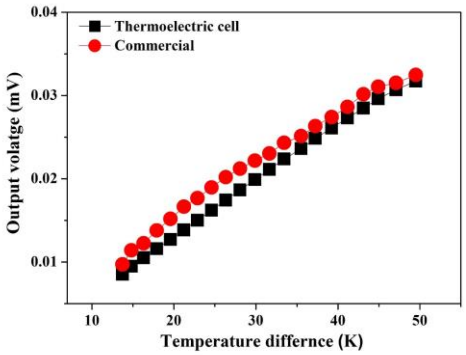

Fig. 9 The different temperature dependence on output voltage of the thermoelectric cell together with commercial

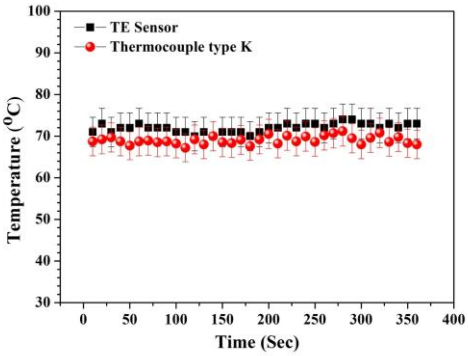

Fig. 10 Time dependent on thermal sensor of the device compared with thermocouple K type

Conclusion

We investigated the crystal structure and TE properties of p-$Bi_{0.4}Sb_{1.6}Te_{3.4}$ and n-Bi_2Te_3 bulk samples applied to new thermoelectric sensor. The thermal sensor was fabricated by a p-$Bi_{0.4}Sb_{1.6}Te_{3.4}$ and n-Bi_2Te_3 couple and compared with thermocouple type K. It was found the good signal of thermal sensor similarly standard of thermocouple type K.

Acknowledgments

This work was supported by Thermoelectric Research Laboratory (TRL), Center of Excellence on Alternative Energy (CEAE), and Research and Researchers for Industry (RRi) find number MSD59I0075, Assoc. Prof. Dr. Tosawat Seetawan, Dr. Kunchit Singsoog and Thailand Research Fund (TRF) Research Career Development Grant, RSA (RSA6180070).

References

[1] Z. Ren, A.A. Taskin, S. Sasaki, K. Segawa, Y. Ando, Optimizing $Bi_{2-x}Sb_xTe_{3-y}Se_y$ solid solutions to approach the intrinsic topological insulator regime. Phys. Rev B. Lett. 84 (2011), 165311.

[2] L.D. Zhao, V.P. Dravid, M.G. Kanatzidis, The panoscopic approach to high performance thermoelectrics. Energy & Environ. Sci. Lett. 7 (2014) 251 – 268.

[3] T. Caillat, M. Carle, P. Pierrat, H. Scherrer, H. Scherrer, S. Scherrer, Thermoelectric properties of $(BixSb_{1-x})_2Te_3$ single crystal solid solutions grown by the T.H.M. method. J. Phys. Chem. Solids. 53 (1992) 1121 – 1129.

[4] D.M. Rowe, Thermoelectric Handbook: Macro to Nano, 2005.

[5] Y. Feutelais, B. Lendre, N. Rodier, V. Agafonov, A study of the phases in the bisnuth-telluride system. Mat. Res. Bull. 50 (1993). 591 – 596.

[6] D. Li, R.R. Sun, X.Y. Qin, Thermoelectric properties of p-type $(Bi_2Te_3)_x(Sb_2Te_3)_{1-x}$ prepared by spark plasma sintering. Intermetallics 19 (2011) 2002 – 2005.

[7] L. Hu, T. Zhu, X. Liu, X. Zhao, Point defect engineering of High-performance bismuth-telluride-based thermoelectric materials. Materials. Adv. Funct. Mater 24 (2015) 5211 – 5218.

[8] B. Pouel, Q. Hao, Y. Ma, Y. Lan, A. Minnich, B.Y. u, X. Yiao, D. Wang, A. Muto, D. Vashaee, X. Chen, J. Liu, M.S. Dresselhaus, G. Chen, Z. Ren, High-thermoelectirc performance of nanostructured bismuth antimony telluride bulk alloy. Science 320 (2015) 634 – 638.

[9] W. Xie, X. Tang, Y. Yan, Q. Zhang, T.M. Tritt, Unique nanostructures and enhanced thermoelectric performance of melt-spun BiSbTe alloys. Appl. Phys. Lett. 94 (2009) 102111.

[10] S.I. Kim, K.H. Lee, H.A. Mun, H.S. Kim, S.W. Hwang, J.W. Roh, D.J. Yang, W.H. Shin, X.S. Li, Y.H. Lee, G.J. Snyder, S.W. Kim, Dense dislocation arrays embedded in grain boundaries for high-performance bulk thermoelectrics. Science. Lett. 348 (2015) 109 – 114.

[11] H. Liu, Y. Wang, D. Mei, Y. Shi, Z. Chen, Design, of a wearable thermoelectric generator for harvesting human body energy. Electrical Engineering. (2016) 55 – 66.

[12] J.J. Kuchle, N.D. Love, Self-powered wireless thermoelectric sensors. Measurement. Lett. 47 (2014) 26 – 32.

[13] Z. Yi, X. Liao, H. Wu, Analysis and experiment of temperature effect on the thermoelectric power sensor. Sensors and Actuators A. Lett. 224 (2015) 99 – 105.

[14] Y.J. Kim, H.M. Gu, C.S. Kim, H. Choi, G. Lee, S. Kim, K.K. Yi, S.G. Lee, B.J. Cho, High-performance self-powered wireless sensor node driven by a flexible thermoelectric generator. Energy. Lett. 162 (2015) 526 – 533.

[15] H. Cheng, Y. Du, B. Wang, Z. Mao, H. Xu, L. Zhang, Y. Zhong, W. Jiang, L. Wang, X. Sui, Flexible Cellulose-based Thermoelectric Sponge towards Wearable Pressure Sensor and Energy Harvesting. Chemical Engineering Journal. Lett. 388 (2018) 1 – 7.

[16] G.E. Lee, I.H. Kim, Y.S. Lim, W.S. Seo, B. Jun, C. Chang, W. Hwang, Preparation and thermoelectric properties of Bi_2Te_3-Bi_2Se_3 Solid Solutions. Journal of the Korean Physical Society. Vol. 64 (2014) 1416 – 1420.

[17] M.G. Asinelli, M.S. Serra, J.M. Marimòn, J.S. Espaulella, The smARTS_Museum_V1: An open hardware device for remote monitoring of Cultural eritage indoor environments. HardwareX. Lett. 4 (2018) e00028.

[18] M.F. Eliana, V.J. Figueira, A.L. Pires, J. Grilo, M.F. Silva, A.M. Pereira, L.M. Goncalves, Enhanced thermoelectric properties of Sb_2Te_3 and Bi_2Te_3 films for flexible thermal sensors. Journal of Alloys Compounds. Lett. 774 (2018) 1102 – 1116.

[19] X. Fan, F. Yang, Z. Rong, X. Cai, G. Li, Characterization and thermoelectric properties of $Bi_{0.4}Sb_{1.6}Te_3$ nanostructured bulk prepared by mechanical alloying and microwave activated hot pressing. Ceramic International. Lett. 41 (2015) 6817 – 6823.